Sources, fate and pathways of Leeuwin Current water in the Indian Ocean and Great Australian Bight: a Lagrangian study in an eddy-resolving ocean model.

Christopher Yit Sen Bull [1] and Erik van Sebille [1, 2]

[1] ARC Centre of Excellence for Climate System Science & Climate Change Research Centre, University of New South Wales, Sydney, Australia.

[2] Grantham Institute & Department of Physics, Imperial College London, London, United Kingdom.

Key Points

1. The Leeuwin Current gets 60-78% of its water from northern sources
2. Large exchanges of water from all sources in the Leeuwin Current region
3. A Lagrangian analysis of pathways quantifies ‘zipper’ effect downstream

Abstract

The Leeuwin Current is the dominant circulation feature in the eastern Indian Ocean, transporting tropical and subtropical water southward. Whilst it is known that the Leeuwin Current draws its water from a multitude of sources, existing Indian Ocean circulation schematics have never quantified the fluxes of tropical and subtropical source water flowing into the Leeuwin Current. This paper uses virtual Lagrangian particles to quantify the transport of these sources along the Leeuwin Current's mean pathway. Here, the pathways and exchange of Leeuwin Current source waters across six coastally bound sectors on the south-west Australian coast are analysed. This constitutes the first quantitative assessment of Leeuwin Current pathways within an offline, 50-year integration time, eddy-resolving global ocean model simulation. Along the Leeuwin Current's pathway we find a mean poleward transport of 3.7 Sv in which the tropical sources account for 60-78% of the transport. Whilst the net transport is small, we see large transports flowing in and out of all the offshore boundaries of the Leeuwin Current sectors. Along the Leeuwin Current's pathway, we find that water from the Indonesian Throughflow contributes 50-66% of the seasonal signal. By applying conditions on the routes particles take entering the Leeuwin Current, we find particles are more likely to travel offshore north of 30°S, while south of 30°S particles are more likely to continue downstream. We find a 0.2 Sv pathway of water from the Leeuwin Current's source regions, flowing through the entire Leeuwin Current pathway into the Great Australian Bight.

1 Introduction

The surface Leeuwin Current is a globally unique eastern boundary current, flowing poleward year round [*Smith et al.*, 1991], it transports fresh, warm water into the West and South Australian coastlines [*Waite et al.*, 2007]. An observationally based study [*Ridgway and Condie*, 2004] showed that the surface Leeuwin Current is the western part of a 5500 km system of currents originating at the North West Cape of Australia (114°E, 22°S) and extending to the southern tip of Tasmania (approx. 146°E, 44°S). However, the circulation off the western coast of Australia is more complicated than a continuous coastal flow confined to the continental slope. Compared to other eastern boundary currents, the Leeuwin Current is rich in eddy activity [*Feng et al.*, 2005]; mesoscale eddies generated from mixed barotropic and baroclinic instability play an important role in transporting heat and salt offshore [*Morrow et al.*, 2003]. Moreover, the Leeuwin Current is not the only named current in the region. Slightly farther offshore and deeper than the surface Leeuwin Current flows the Leeuwin undercurrent, an equatorward flowing subsurface current [*Woo and Pattiaratchi*, 2008]. Inshore of the surface Leeuwin Current are the summer only, wind driven equatorward Ningaloo Current and Capes Current, located between 22-24°S [*Woo et al.*, 2006] and 33-34°S [*Pearce and Pattiaratchi*, 1998; *Gersbach et al.*, 1999], respectively.

The surface Leeuwin Current is an important pathway for water originating in the Pacific Ocean to enter into Australia's boundary current system. Since *Kundu and McCreary* [1986] it has been suggested that the Leeuwin Current, via the Indonesian Throughflow, provides a pathway for water coming from the Pacific

Ocean into western Australia's coastlines. A more recent Lagrangian modelling study [*Domingues et al.*, 2007] confirmed this general pathway, but the quantitative contribution of this source remains unclear [*Furue et al.*, 2013]. In the context of the recent warming air temperature hiatus, the Indonesian Throughflow has transported 70% of the Pacific Ocean's anomalous heat in the past decade into the upper 700m of the Indian Ocean [*Lee et al.*, 2015]. The multi-decadal trend in stronger Pacific trade winds corresponds to stronger Leeuwin Current transport [*Feng et al.*, 2011] and is a contributing factor to the unprecedented 2011 marine heat wave off Western Australia [*Feng et al.*, 2013; *Benthuysen et al.*, 2014]. Thus, to understand the regional impact of the anomalous ocean heat in the Indian Ocean and identify/characterise Australia's extreme ocean warming events in the future, a more thorough understanding of the Leeuwin Current's tropical sources is needed.

The surface Leeuwin Current is also an important component of the large scale circulation in the Indian Ocean. Using a five year POP11B model simulation with a Lagrangian framework where water parcels are tracked, *Domingues et al.* [2007] found that water leaving the Indonesian Throughflow exits in the South Java Current and then returns eastward in the Eastern Gyral Current. *Domingues et al.* [2007] found an additional tropical source region for the Leeuwin Current, that is, water flowing from the equatorial Indian Ocean via the South Java Current. From the subtropical Indian Ocean, *Domingues et al.* [2007] found water entering the Leeuwin Current via the southern branch of the South Indian Countercurrent (SICC) (terminology from [*Menezes et al.*, 2014b]). More recently, *Menezes et al.* [2014b] has better resolved the SICC, this work suggests that the central branch of the SICC is also a source for the Leeuwin Current. These pathways have been corroborated observationally, examples include the use of in situ observations [*Woo and Pattiaratchi*, 2008; *Xu et al.*, 2015], Argo-based atlases and satellite data [*Menezes et al.*, 2013, 2014b]. Whilst the aforementioned studies describe the circulation of the region, they do not quantify the relative contributions of the different surface Leeuwin Current sources to the mean flow [*Furue et al.*, 2013].

Understanding of the fate of Leeuwin Current water is even more limited than that of its sources. Whilst the Leeuwin Current extends to around 300m [*Feng*, 2003], surface observations might give some insight into the fate of Leeuwin Current water. *Ridgway and Condie* [2004], however, when looking for surface drifters that had advected from the Leeuwin Current proper into the Great Australian Bight noted there was 'no single period in which drifters were deployed over the entire current path'. Due to this lack of observations, it is not well known how much water flows from the Leeuwin Current into the Great Australian Bight as compared to flowing offshore into the Indian Ocean.

Although there is a lack of quantitative estimates of the Leeuwin Current's water pathways, there are observationally based Eulerian estimates of transport across Leeuwin Current sections. An observationally based study by *Feng* [2003] found southward transports at 32°S of 3.4 Sv, 3.0 Sv and 4.2 Sv for the mean, El Niño and La Niña years respectively. Recent work by Ridgway and Godfrey [2015] suggests that the source of the Leeuwin Current's seasonal cycle is an annual sea level signal starting in the Gulf of Carpentaria in November and travelling around Australia's coast as far as Tasmania by July. The seasonal variability of the Leeuwin Current is well established [*Ridgway and Condie*, 2004; *Meuleners et al.*, 2007; *Waite et al.*, 2007; *Hendon and Wang*, 2009]. The current is strongest in Austral winter when equatorward winds are weakest [*Smith et al.*, 1991; *Meuleners et al.*, 2007; *Hendon and Wang*, 2009]. In the most extensive field study to date, *Smith et al.* [1991] calculated the Leeuwin Current's alongshore southward transport at 29.5°S as ranging from< 2 Sv in February to >6 Sv in March and June.

The aims of this study are twofold. First, to quantify tropical and subtropical source exchanges in the Leeuwin Current. Specifically, we quantify how much water comes from the tropical Indonesian Throughflow, the tropical equatorial Indian Ocean and the subtropical interior western Indian Ocean. Second, to quantify the amount of water that goes into the Great Australian Bight compared to the amount of water that recirculates offshore into the Indian Ocean. Both of these questions will be addressed using a Lagrangian framework in the context of a 1/10° global ocean model over a fifty year time series.

This study builds on the aforementioned previous Lagrangian study [*Domingues et al.*, 2007] in a number of ways. Specifically, we use finer temporal resolution, namely five days compared to twenty days, and we study a longer temporal extent, namely fifty years compared to five years. As a result we are able to consider long term Leeuwin Current pathways and the seasonal cycle. Similarly, as our experiment is run offline we are able to track significantly more particles allowing for quantitative inferences. In addition, by defining sectors along the south west Australian coastline this work quantifies source exchange fluxes, source pathways and the seasonal cycle across and alongshore the south west Australian coastline. Finally, having a longer time series and a Lagrangian framework allows us to examine the fate of Leeuwin Current water farther downstream. Thus, this study extends the previous work by calculating transports and pathways associated with different Leeuwin Current sources.

The paper is organised as follows. Section 2 describes the ocean model, Lagrangian framework and definition of the Leeuwin Current sectors used in this paper. Results are examined in section 3. Section 4 provides a summary and comparison of results, closing with a discussion of the limitations of the work, its broader importance and suggestions for future work.

2 The Model and Methods

2.1 Ocean General Circulation Model

In this study, the sources and destinations of Leeuwin Current water are studied using the high-resolution TROPAC01 model. This model configuration, developed by the European Drakkar cooperation [*Barnier et al.*, 2007], is based on NEMO [*Madec*, 2008] code. It is a 1/10° horizontal resolution model of the tropical Indo-Pacific region (73°E–63°W to 49°S–31°N), nested within a half-degree global ocean/sea-ice model. In the vertical, TROPAC01 has 46 z-levels: 10 levels in the top 100m and a maximum layer thickness of 250m at depth, whereby bottom cells are allowed to be partially filled [*Barnier et al.*, 2007]. The COREv2-IA atmospheric forcing is used in this study, it has been designed to aid our understanding of the observed ocean record and has broad usage with global ocean-ice models as established by the Coordinated Ocean-ice Reference Experiments [*Griffies et al.*, 2009]. The atmospheric forcing builds on the CORE reanalysis products developed by *Large and Yeager* [2008] covering the period 1948–2009 and is applied via bulk air-sea flux formulae. The TROPAC01 simulation uses laterally spatially varying eddy coefficients, namely, a Laplacian operator for iso-neutral diffusion of tracers and a bi-laplacian operator for lateral diffusion of momentum. TROPAC01 is run with a prognostic turbulent kinetic energy scheme [*Gaspar et al.*, 1990] for vertical mixing. Further details in *Madec* [2008]. For the analysis, 50 years (1960–2009) of data from the TROPAC01 hind-cast experiment will be used, with temporal means available every 5 days. The combination of output every five days, over a long time series with eddy-resolving resolution enables us to address a range of questions on different temporal and spatial scales.

With reasonable accuracy, the model reproduces the major circulation features in the region. This is evident when comparing the overlapping time period of 1993–2009 in terms of simulated sea-surface height with AVISO altimetry data (Figure 1). In *van Sebille et al.* [2014], using the same model, the authors note an extended tongue of elevated sea surface height in the model Indian Ocean at around 15°S, which is confined to the far eastern basin in the altimetry data. We can see that other biases in our region of interest are relatively small, except for the slightly higher sea surface height values very close to the coast. The variability of sea surface height in the model is also in good agreement when compared to altimetry (Figure 1d-e), we see the south Indian Ocean is eddy rich (e.g. [*Feng et al.*, 2005]). As *van Sebille et al.* [2014] noted, TROPAC01 tends to underestimate more energetic regions (Figure 1f) with the exception of coastal areas. These coastal discrepancies (Figure 1c and Figure 1f), may be due to satellite performance deteriorating near coastal areas [*Saraceno et al.*, 2008] and therefore do not necessarily imply the model is doing a poor job.

2.2 Eulerian TROPAC01 validation at 32°S

As we are particularly interested in water transport in the Leeuwin Current region, we validate TROPAC01 against [*Feng*, 2003]. To minimise the effect of interannual variability, throughout this subsection we use TROPAC01's entire timeseries 1960-2009. In *Feng* [2003], Leeuwin Current variability (offshore of Fremantle) was reconstructed using a range of observations including Fremantle sea level and temperature/salinity records near Rottnest Island. TROPAC01's (Eulerian) mean and bimonthly mean velocity fields in Figure 2 may be compared to the geostophic velocities in Figure 6d and Figure 7c of [*Feng*, 2003] (respectively). From Figure 8 of [*Feng*, 2003] we know that the southward Ekman transport across this section is low and so its contribution to Figure 2 would be small. Figure 2 shows that along 32°S, like in [*Feng*, 2003], the core of the Leeuwin Current is at 115°E and the velocity core tilts slightly toward the coast with increasing depth.

The bimonthly means in Figure 2 show that TROPAC01 performs well, qualitatively; in the summer months we see the characteristic weakening of the Leeuwin Current, as we approach the winter months we can see the expected deepening and widening of the core of the Leeuwin Current. Quantitatively, in both figures the flow speeds are lower than the observed values but we notice that this effect on transport is cancelled out by the flow being broader (Figure 2). Depth integrating from 110°E to the continental edge at 32°S down to 270m gives a transport estimate of 2.9 Sv, this compares well with [*Feng*, 2003] of 3.4 Sv.

Figure 3 shows how well TROPAC01 reproduces the seasonality of the Leeuwin Current. We compare the monthly mean Eulerian transport between 1960-2009 in TROPAC01 at 32°S with *Feng's* [2003] (Figure 8) mean for years 1950-2000 at 32°S. This and the depth integration done above are typical means of validation for a model's transport for the Leeuwin Current (e.g. [*Smith et al.*, 1991; *Feng et al.*, 2008; *Hendon and Wang*, 2009; *Benthuysen et al.*, 2014]). Given the different time periods, the agreement in Figure 3 is quite good, the seasonal cycle is captured well and the timing of the winter intensification of the Leeuwin Current agrees well with observations (e.g. [*Feng*, 2003]). Indeed, TROPAC01 has improved its representation of the seasonal cycle since previous versions of the model. In *Feng et al.* [2008] fields from the ORCA025-KAB001 (ORCA025) 0.25° model were analysed in the Leeuwin Current region. ORCA025 is an earlier version of TROPAC01 and used the same atmospheric forcing. Comparing Figure 3 here with Figure 5 from *Feng et al.* [2008], we see that the higher resolution TROPAC01 has increased summer transport and an improved timing of winter intensification; two issues *Feng et al.* [2008] raised when validating the earlier ORCA025 version of TROPAC01.

2.3 The Lagrangian particle model and setup

The Leeuwin Current sources, pathways and associated transports can most aptly be studied by tracking virtual Lagrangian particles in model velocity fields (e.g. [*van Sebille et al.*, 2013]). We use the Connectivity Modelling System (CMS) v1.1 [*Paris et al.*, 2013] to integrate the virtual particles in the three-dimensional time-evolving flow.

As the focus is on the region around Australia, only data in a subdomain between 90°E–190°E and 49°S–15°N is used (pictured in Figure S1). Using the TROPAC01 dataset to track water masses into the Leeuwin Current, we release particles in the following known Leeuwin Current source regions. Specifically:

1. The *Indonesian Throughflow region* consisting of two zonal release sections and one meridional release section. A Karimata Strait release section at 4°S between 106-114.5°E with 0.1° horizontal spacing and 10 m vertical spacing. Another zonal section in Makassar and Moluccas Straits at 4°S between 115.6-134.6°E with 0.1° horizontal spacing and 50 m vertical spacing. A Torres Strait meridional release section along 142.5°E between 9.3-10.7°S with 0.1° horizontal spacing and 10 m vertical spacing. The vertical spacing in Karimata and Torres Strait have been reduced to accommodate for shallow bathymetry.
2. The *northern offshore* section: a zonal section at 4°S between 90.0-102.25°E with 0.25° horizontal spacing and 50 m vertical spacing.

1. The *western offshore* section: A meridional section along 90°E between 4-49°S with 0.5°degree horizontal spacing and 50 m vertical spacing.

These release sections are pictured in Figure S1, supplementary material. Maps of depth-integrated transport in Sverdrup into the Leeuwin Current region from each of the Indonesian straits, Torres Strait and both offshore Indian releases are shown in Figure S2.

As the objective of the present work is to identify source contributions to the Leeuwin Current's mean flow, particles will not be allowed north of 4°S or west of 90°E. Meaning, once a particle crosses either of these lines, it is removed from the experiment from that point on. Particles are released every five days down to a depth of 1075 metres (where bathymetry allows). This is more than sufficient depth as both the South Indian Countercurrent and Leeuwin Current system do not extend below 1000 m [*Siedler et al.*, 2006; *Waite et al.*, 2007]. Since this study's focus is on Leeuwin Current trajectories, particles are only released if they have an initial southward/eastward trajectory for zonal/meridional sections, respectively. These three release sections equate to a tracking of 4.8 million particles.

Particle trajectories need to account for the ramp-up effect [*van Sebille et al.*, 2012, 2014], namely the time it takes for water to reach the south-eastern end of the Leeuwin Current region from the release locations. Specifically, out of all three releases, the water coming from the western offshore section takes the longest to be advected through the Leeuwin Current region. The distribution of transit times of western offshore particles suggests a ramp up time of ~6 years. This comes from the amount of time it takes 90% of the particles from the western offshore release section to arrive at the farthest area of interest in this paper: the Great Australian Bight. For this reason, for the remainder of this paper, across all sources, particles released between 1960-2003 that arrive in the Leeuwin Current region after 1965 are analysed.

The particles are assigned a transport equal to the local velocity in the release grid cell times the area of that grid cell. The length of the release grid cell in this experiment varies on the release section, the release grid cell for each release section can be found in the release definitions above. The particles are then tracked forward in time until they reach one of the domain boundaries or until the end of the time series. Along a particle's trajectory, the particle maintains its original transport; this method has been used successfully by others, for example see [*Döös*, 1995; *Speich et al.*, 2002; *van Sebille et al.*, 2010, 2012]. This method has recently been validated in the Indonesian archipelago, yielding transports that agree strongly with their Eulerian analogue [*van Sebille et al.*, 2014]. Furthermore, this last paper demonstrated TROPAC01's capacity to simulate a realistic Indonesian Throughflow, which is important for the present work as the Leeuwin Current is partially forced by the Indonesian Throughflow [*Furue et al.*, 2013; *Schloesser*, 2014]. Previous versions of TROPAC01 have also been validated in a variety of ways in terms of the Leeuwin Current and Indonesian Throughflow [*Feng et al.*, 2008, 2011; *Schwarzkopf and Böning*, 2011].

2.4 Defining six coastally bound sectors along the south-west Australian coast

Since we are interested in the water mass source exchanges in the Leeuwin Current region, we define six adjacent sectors along the south-western coastal boundary of Australia (see black lines Figure 5). For the remainder of this paper, the sectors will be numbered 1-6 starting upstream in the northwest and then moving downstream south and east (as numbered in Figure 5). Studies such as [*Smith et al.*, 1991; *Feng et al.*, 2008; *Benthuysen et al.*, 2014] suggest that the Leeuwin Current's mean flow does not meander beyond 200-300 km offshore.

3 Results

3.1 Particle connectivity from the Pacific Ocean and equatorial Indian Ocean to south western Australia

Figure 4 maps the proportion of transport in each 0.5° grid cell that enter the Leeuwin Current. Dark blue regions indicate that all particles (100%) that visit those grid cells pass through the Leeuwin Current at some point along their trajectories, while dark red regions indicate no particles (0%) visit the Leeuwin Current. Here, particles are defined to visit the Leeuwin Current region when they enter any of the six sectors defined in section 2.4 (black lines on Figure 4). As this section focuses on the tropical sources of the Leeuwin Current, Figure 4 does not consider particle trajectories from the western offshore source. Cells that are unshaded indicate grid cells where no trajectories entered.

Using Lagrangian trajectories, Figure 4 highlights the northern regions in the southeast Indian Ocean that are connected by the Leeuwin Current. Grid cells south of the 50% contour are dominated by particles bound for or coming from the Leeuwin Current region. The tongue of blue contours extending along the northwest shelf of Australia indicates that once water is near the northwest shelf of Australia it is likely to enter the Leeuwin Current region. Indeed, at approximately 19.5°S, 118.5°E the 100% contour indicates that any particle in that location will enter the Leeuwin Current region (or has come from there). Similarly, comparing water southeast and west of the Indonesian Aru Islands (134°E), water on the south eastern side is more likely to end up in (or come from) the Leeuwin Current region. From Figure 4 we can conclude that within the domain presented, on the timescales available in the model, the only way for water originating in the low latitudes to get to mid-latitude and South Australia is to pass through the Leeuwin Current region. Thus, as expected the Leeuwin Current is the only western Australian pathway for water travelling from the tropical Pacific Ocean/equatorial Indian Ocean to mid-latitude and southern Australia.

3.2 Mean and seasonal source water exchanges in the Leeuwin Current region.

Figure 5 addresses a key objective of this paper, to quantify the tropical and subtropical source exchange in the Leeuwin Current region. Specifically, we have depth-integrated the Lagrangian transports (in Sv) from the surface to 300m across the borders of the (pictured) sectors, taking the mean over 1966-2003 (a date range shorter than the available model data, due to 'ramp-up effect', see section 2.3). The colour of the arrows represent the three different particle source releases (section 2.3): orange arrows are particles originating from the

Indonesian Throughflow region, purple arrows are for the northern offshore release and green arrows for the western offshore release. See section 2.3 for the formal definition of these releases. This colouring scheme persists for Figure 6 and Figure 7. Size and direction of arrows are indicative of transport size and direction of flow (respectively). The sectors in Figure 5 have arrows in both directions as particles are allowed to circulate freely in the domain. We define *downstream flow* to mean the southward crossing of sectors 1/2/3 and eastward bound water for sectors 4/5/6 (as numbered in Figure 5). Figure 6 and Figure 7 examine only the downstream flow. Reference to the *Leeuwin Current's extension* is meant to be any Leeuwin Current water rounding Cape Leeuwin heading east into sectors 5 and 6.

The combined downstream alongshore transports in Figure 5 gives transport estimates of 3.6, 3.2, 3.9, 4.2, 3.9, 4.3, 2.8 Sv. These transports can be interpreted as the Lagrangian analogue of transport for the Leeuwin Current from observationally based studies (e.g. [*Smith et al.*, 1991; *Feng*, 2003]). The net southward transport of sectors 2 and 3 from Figure 5 compare favourably with *Feng's* [2003] observationally based estimate of 3.4 Sv at 32°S.

Since we are using a Lagrangian framework, these transports can be broken up in terms of their origin. The northern sources (orange/purple) account for 60-78% of the water found in the downstream flow of the Leeuwin Current. Along the downstream flow, the Indonesian Throughflow source (orange) is the largest, followed by the western offshore source (green) and then the northern offshore source (purple). Also along the downstream flow, aside from the poleward fluxes exiting sector 2, the western offshore fluxes (green) are 2-3 times bigger than the northern offshore fluxes (purple). The transports from the western offshore source are significant in magnitude, but water from this source is slightly deeper and less well mixed than the northern sources (Figure 7).

Whilst the mean flow of the Leeuwin Current is poleward, Figure 5 reveals significant exchange across the outside boundaries of the sectors, particularly from the western offshore water (purple). The net transports, however, are a small fraction compared to the eastward and westward flows, individually. This is indicative of the eddy rich region west of the mean Leeuwin Current pathway (see Figure 1e and [*Morrow et al.*, 2004; *Feng et al.*, 2005]). These transport results are interesting as observational data across these boundaries is quite sparse. As *Menezes et al.* [2014a] highlight 'the South Indian Ocean is historically poorly observed on a basin scale', this can be seen clearly in Figure 3.A.2 in [*Rhein et al.*, 2013]. Historically, most observations of transport have been taken perpendicular to the coast (e.g. [*Woo and Pattiaratchi*, 2008]).

In section 2, it was shown that TROPAC01 captures the Leeuwin Current's seasonal cycle reasonably well. In 2004, *Ridgway and Condie* [2004] demonstrated how the seasonality of the Leeuwin Current affects sea surface temperatures. What has not been quantified is the contribution of the Leeuwin Current's different sources to the seasonal cycle, this is presented in Figure 6. Looking at the crossings at 26°S, 30°S and 34°S (Figure 6a-c) the peak transport occurs in different months. In the 26°S and 34°S crossings (Figure 6a, c) maximum transport occurs in March and April, respectively. The maximum at

30°S (Figure 6b) in July compares favourably with the maximum observed by *Smith et al.* [1991] at Dongara (29.5°S) in June. *Smith et al.* [1991] measured a geostrophic transport range of 2 Sv (February 1987) to more than 5 Sv (March, June and August 1987) at Dongara (29.5°S), whilst the summer transports in Figure 6b are higher, given the different sampling periods and location this appears to be in reasonable agreement with Figure 6b. In the Leeuwin Current extension we see that the peak transport occurs consistently in May. The strongest downstream flow month is in May, across 120°E (Figure 6e), which is due to the western offshore section contributing more (compare Figure 6d and Figure 6e). The largest seasonal variability is also at 120°E with an approximate 4 Sv difference between January and May. A number of papers on the Leeuwin Current have shown a seasonal southward propagating sea surface height signal for example Figure 5 in [*Ridgway and Godfrey*, 2015] and Figure 3 in [*Ridgway and Condie*, 2004]. In contrast, a similar signal is not found from the Lagrangian transport sections plotted in Figure 6. This somewhat surprising discrepancy may be a deficiency of the TROPAC01 simulation and is possibly caused by the sea surface height bias in the model Indian Ocean (around 15°S) discussed in section 2.1.

The relative contributions of each source and their seasonal cycle vary at each crossing. Across all crossings, the Indonesian Throughflow region source (orange) has the most seasonal variability, followed by the western offshore source (green). Since the northwest Indian Ocean's contribution is small and has little seasonality, it is the seasonality of the western offshore source and Indonesian Throughflow (including Torres Strait) that contribute the seasonality of the total. Indeed, the Indonesian Throughflow region contributes 66%, 56%, 53%, 51%, 50% and 53% of the total transport to the crossings in Figure 6a-f, respectively. Figure 6 supports *Ridgway and Godfrey* [2015] recent work on the source of the Leeuwin Current's seasonality, specifically Figure 6 shows that advective processes from the Leeuwin Current's tropical sources contribute to the seasonal cycle of the Leeuwin Current. As discussed in the introduction, the Lagrangian framework provides an opportunity to track the mixing of source waters along the Leeuwin Current's downstream pathway. Figure 7 is a series of depth-horizontal coordinate space plots for the sector crossings along the downstream flow for the mean over 1966-2003. Along the downstream flow (all plots in Figure 7) the core regions of the northern sources (orange and purple) are almost coincident. The western offshore source (green) has a core that is slightly deeper than the other two sources, so it follows that transport from the northern sources is closer to the shelf. The Indonesian Throughflow region (orange) contributes slightly more transport near the shelf than any other source. The location of the core at 30°S agrees well with the core location of the mooring at 29.5°S in [*Smith et al.*, 1991]. In sectors 4-6 (Figure 7d-f), along the Leeuwin Current extension, all three sources steadily shallow and the core regions continue to merge.

3.3 Particle Connectivity in the Indian Ocean and Great Australian Bight

A number of papers suggest that the Leeuwin Current is part of a continuous 5500 km coastal current system (e.g. [*Ridgway and Condie*, 2004; *Batteen and Miller*, 2009; *Ridgway and Godfrey*, 2015]). Whilst these studies have successfully tracked sea surface height/temperature anomalies around the Australian coast, it has not been clear how much water makes it directly from the source regions to the Great Australian Bight. Lagrangian tracking of water parcels provides an opportunity to quantify how these regions are connected by advection. To address this question, Figure 8 is different to Figure 5, Figure 6 and Figure 7; particles must meet strict criteria for their flux to be shown. Particle trajectories in Figure 8 will therefore be labelled as *conditional pathways*. Specifically, the conditions applied are as follows: the particle's trajectory must enter by the first sector and recirculating particles are not counted. Thus, this figure is a quantification of direct pathways through the Leeuwin Current region. The bold end of each edge indicates the direction of flux and inshore green edges indicate water that is travelling close to the coast having passed through all preceding inshore sector(s). For example, a flux of 0.7 Sv on the third green edge indicates transport from particles that have travelled directly through the first two sectors and are now crossing into the third sector. The flux itself is thus interpreted as the volume of water undertaking that pathway over the mean of the time series. Offshore red edges quantify trajectories that travelled through all green inshore upstream sector(s) and then exited the system via the red offshore edge. Finally, purple curved edges indicate trajectories that have travelled directly through the previous inshore sector(s) and then recirculated upstream. Units are in Sv and the mean is taken over the years 1966-2003 and depth-integrated to 300m.

This figure addresses the second key objective of this paper, to quantify the amount of water that goes into the Leeuwin Current's extension compared to the amount of water that moves offshore into the Indian Ocean. Looking at the first sector, the flux going offshore (red edge) is larger than the flux going downstream (green edge). From the second sector particles heading offshore and downstream are approximately equal, and by the third sector more particles continue downstream than flow offshore. This partitioning then continues for the remainder of the downstream sectors. In other words, once a particle has gone through the first three sectors directly, it is likely to continue around Cape Leeuwin into the Great Australian Bight. Looking at the purple edges, it is clear that recirculating particles make up a very small fraction of the particle pathways. Sources have been combined in Figure 8 as there is little difference in the pathway taken when comparing source. The exception to this is the western offshore particles, Figure S3 shows that very few particles from the western offshore section follow the mean Leeuwin Current pathway. When compared to particles from the two northern sections, Figure 7 shows that western offshore particles are further offshore and so are less influenced by bathymetry. There are likely a number of processes that influence the pathway of the western offshore particles; *Menezes et al.* [2014b] discuss the dynamics that influence the flow patterns of the basin wide flows in detail.

Comparing these conditional pathways to the unrestricted particles in Figure 5, it is clear that the fluxes in the downstream sectors are much smaller when re-circulating particles are not allowed. In other words, Figure 8 shows that compared to the unrestricted pathways across the same sectors in Figure 5, very little water actually travels the full length of the Leeuwin Current and then around Cape Leeuwin into the Great Australian Bight directly.

4 Conclusions and Discussion

By tracking virtual Lagrangian particles in the eddy-resolving TROPAC01 model, we have quantified the fluxes of source waters and major pathways through the Leeuwin Current region. The Lagrangian framework has provided an insight into the connectivity between the tropical and subtropical sources of the Leeuwin Current and the Great Australian Bight. Indeed, if we take the particles from all the northern releases that have and have not entered any of the sectors and plot their proportion of transport (Figure 4), then we see that, within the model domain, the only way to reach the Great Australian Bight is via the Leeuwin Current.

Along the Leeuwin Current's pathway, we find water originating from the northern releases to be the most important, accounting for 60-78% of the transport; corroborating the traditional view that the Leeuwin Current is principally sourced from the Indonesian Throughflow, Torres Strait and the tropical Indian Ocean. Nevertheless, we also find large exchanges from all sources across the outside boundaries of the sectors; this includes water sourced from the interior Indian Ocean (the western offshore source). As the Leeuwin Current gains strength over winter (Figure 6), we see that water coming from the Indonesian Throughflow dominates the seasonal cycle.

Whilst thinking about the kinds of eddies that are resolved in a 1/10° model with output every five days we ask the following question. What portion of the fluxes in Figure 5 are attributable to water recirculating in large eddies? We address this by reproducing Figure 5 and only considering particles that transit directly through the sectors, in order from northwest to southeast, removing times a particle crosses a boundary more than once (Figure 8). Figure 8 indicates that significant amounts of the fluxes in Figure 5 are from recirculating particles or particles that did not start in sector 1 and flow directly through the sectors. In the sectors downstream of Cape Leeuwin, Figure 8 when compared to Figure 5 indicates that relatively little water travels directly from the start of the Leeuwin Current into the Great Australian Bight.

These differences between the non-conditional and conditional pathway analyses exemplify the non-laminar pathways in the Leeuwin Current region. This is important for two reasons. Firstly, it indicates the importance of eddies causing particles to recirculate. Secondly, it shows the relatively small number of particles that navigate the direct route along the Leeuwin Current and into the Leeuwin Current extension as described by *Ridgway and Condie* [2004]. This study is the first quantitative estimate of transport connecting the tropics and subtropics to the Great Australian Bight via the Leeuwin Current.

A number of studies have shown that the increase in Leeuwin Current transport in La Niña years can have a damaging effect on the temperature sensitive coastlines of western Australia [*Pearce and Feng, 2007; Wernberg et al., 2011; Thompson et al., 2015*]. Whilst beyond the scope of the present work, higher transports along the western Australian coast in La Niña years are expected, with more particles rounding Cape Leeuwin into the Great Australian Bight. Future work could extend this study by quantifying the change in pathways in between El Niño and La Niña years. Building on recent work by *Ayers et al.*

[2014], future work could regionally examine the biological implications of few tracked particles travelling the whole length of the Leeuwin Current into the Great Australian Bight. Recent work by *Wang et al.* [2015] has challenged the conventional view that Leeuwin Current strength is the single indicator of annual catch size of western rock lobster. *Wang et al.* found that cyclonic cold core eddies have a positive effect on the nutritional condition of the larvae, as a result, it would be interesting to track particle exchanges between the Leeuwin Current and Leeuwin Undercurrent.

The results in this paper are based on a single model and so are affected by biases in the forcing, sensitivity to a z-level coordinate system, the resolution of the model and the subsequent processes it can resolve. In section 2.1, biases in TROPAC01's sea surface height were discussed when compared to AVISO. As TROPAC01 tends to underestimate the energetic regions (Figure 1f) it is possible the results in this paper underestimate some of the eddy-driven fluxes. Thus, it is possible other eddy-resolving ocean model simulations using different forcing products would give slightly different results. Although the results in this paper are based purely on a model, they will assist future work in understanding the Leeuwin Current's role in regional climate and circulation in the region. Examples include: marine heatwaves [*Benthuysen et al.*, 2014], connectivity in the region [*Coleman et al.*, 2013], the effects of climate change on Australia's boundary currents [*Sun et al.*, 2012] and understanding the dynamics of the Indian Ocean's anomalous eastward flows [*Menezes et al.*, 2014b].

5 Acknowledgements

Copies of the data used for this study are stored at NCI, more information on the data and how to access it can be found at https://researchdata.ands.org.au/view/?id=472299. The altimeter products were produced by Ssalto/Duacs and distributed by Aviso with support from Cnes. This work was supported by an Australian Postgraduate Award and the Australian Research Council (ARC). Specifically, in the latter case, the ARC Centre of Excellence in Climate System Science and grant DE130101336. TROPAC01 was developed within the framework of the DFG project SFB754 and integrated at the North-German Supercomputing Alliance (HLRN). We thank Helen Phillips for her suggestions on how to improve the manuscript.

6 References

Ayers, J. M., P. G. Strutton, V. J. Coles, R. R. Hood, and R. J. Matear (2014), Indonesian throughflow nutrient fluxes and their potential impact on Indian Ocean productivity, *Geophys. Res. Lett.*, *41*(14), 5060–5067, doi:10.1002/2014GL060593.

Barnier, B. et al. (2007), Eddy-permitting ocean circulation hindcasts of past decades, *CLIVAR Exch.*, *12*, 8–10.

Batteen, M. L., and H. a. Miller (2009), Process-oriented modeling studies of the 5500-km-long boundary flow off western and southern Australia, *Cont. Shelf Res.*, *29*(4), 702–718, doi:10.1016/j.csr.2008.11.011.

Benthuysen, J., M. Feng, and L. Zhong (2014), Spatial patterns of warming off Western Australia during the 2011 Ningaloo Niño: quantifying impacts of remote and local forcing, *Cont. Shelf Res.*

Coleman, M., M. Feng, M. Roughan, P. Cetina-Heredia, and S. D. Connell (2013), Temperate shelf water dispersal by Australian boundary currents: Implications for population connectivity, *Limnol. Oceanogr. Fluids Environ.*, *3*, 295–309, doi:10.1215/21573689-2409306.

Domingues, C. M., M. E. Maltrud, S. E. Wijffels, J. a. Church, and M. Tomczak (2007), Simulated Lagrangian pathways between the Leeuwin Current System and the upper-ocean circulation of the southeast Indian Ocean, *Deep Sea Res. Part II Top. Stud. Oceanogr.*, *54*(8-10), 797–817, doi:10.1016/j.dsr2.2006.10.003.

Döös, K. (1995), Interocean exchange of water masses, , *100*(95), 499–514.

Feng, M. (2003), Annual and interannual variations of the Leeuwin Current at 32°S, *J. Geophys. Res.*, *108*(C11), 3355, doi:10.1029/2002JC001763.

Feng, M., S. Wijffels, S. Godfrey, and G. Meyers (2005), Do Eddies Play a Role in the Momentum Balance of the Leeuwin Current ?, *J. Phys. Oceanogr.*, *35*, 964–975.

Feng, M., A. Biastoch, C. Böning, N. Caputi, and G. Meyers (2008), Seasonal and interannual variations of upper ocean heat balance off the west coast of Australia, *J. Geophys. Res.*, *113*(C12), C12025, doi:10.1029/2008JC004908.

Feng, M., C. Böning, A. Biastoch, E. Behrens, E. Weller, and Y. Masumoto (2011), The reversal of the multi-decadal trends of the equatorial Pacific easterly winds, and the Indonesian Throughflow and Leeuwin Current transports, *Geophys. Res. Lett.*, *38*(11), n/a–n/a, doi:10.1029/2011GL047291.

Feng, M., M. J. McPhaden, S.-P. Xie, and J. Hafner (2013), La Niña forces unprecedented Leeuwin Current warming in 2011., *Sci. Rep.*, *3*, 1277, doi:10.1038/srep01277.

Furue, R., J. P. McCreary, J. Benthuysen, H. E. Phillips, and N. L. Bindoff (2013), Dynamics of the Leeuwin Current: Part 1. Coastal flows in an inviscid, variable-density, layer model, *Dyn. Atmos. Ocean.*, *63*, 24–59, doi:10.1016/j.dynatmoce.2013.03.003.

Gaspar, P., Y. Grégoris, and J.-M. Lefevre (1990), A simple eddy kinetic energy model for simulations of the oceanic vertical mixing: Tests at station Papa and long-term upper ocean study site, *J. Geophys. Res.*, *95*(C9), 16179, doi:10.1029/JC095iC09p16179.

Gersbach, G. H., C. B. Pattiaratchi, G. N. Ivey, and G. R. Cresswell (1999), Upwelling on the south-west coast of Australia—source of the Capes Current?, *Cont. Shelf Res.*, *19*(3), 363–400, doi:10.1016/S0278-4343(98)00088-0.

Griffies, S. M. et al. (2009), Coordinated Ocean-ice Reference Experiments (COREs), *Ocean Model.*, *26*(1-2), 1–46, doi:10.1016/j.ocemod.2008.08.007.

Hendon, H. H., and G. Wang (2009), Seasonal prediction of the Leeuwin Current using the POAMA dynamical seasonal forecast model, *Clim. Dyn.*, *34*(7-8), 1129–1137, doi:10.1007/s00382-009-0570-3.

Kundu, P. K., and J. P. McCreary (1986), On the Dynamics of the Throughflow from the Pacific into the Indian Ocean, *J. Phys. Oceanogr.*, *16*, 2191–2198.

Large, W. G., and S. G. Yeager (2008), The global climatology of an interannually varying air–sea flux data set, *Clim. Dyn.*, *33*(2-3), 341–364, doi:10.1007/s00382-008-0441-3.

Lee, S., W. Park, M. O. Baringer, A. L. Gordon, B. Huber, and Y. Liu (2015), Pacific origin of the abrupt increase in Indian Ocean heat content during the warming hiatus, *Nat. Geosci.*, (May), doi:10.1038/NGEO2438.

Madec, G. (2008), NEMO ocean engine, *Note du Pole modélisation, Inst. Pierre- Simon Laplace (IPSL), Fr.*, (27).

Menezes, V. V., H. E. Phillips, A. Schiller, C. M. Domingues, and N. L. Bindoff (2013), Salinity dominance on the Indian Ocean Eastern Gyral current, *Geophys. Res. Lett.*, *40*(21), 5716–5721, doi:10.1002/2013GL057887.

Menezes, V. V., M. L. Vianna, and H. E. Phillips (2014a), Aquarius sea surface salinity in the South Indian Ocean: Revealing annual period planetary waves, *J. Geophys. Res. Ocean.*, 3883–3908, doi:10.1002/2014JC009935.Received.

Menezes, V. V., H. E. Phillips, A. Schiller, N. L. Bindoff, C. M. Domingues, and M. L. Vianna (2014b), South Indian Countercurrent and associated fronts, *J. Geophys. Res. Ocean.*, *119*(10), 6763–6791, doi:10.1002/2014JC010076.Received.

Meuleners, M. J., C. B. Pattiaratchi, and G. N. Ivey (2007), Numerical modelling of the mean flow characteristics of the Leeuwin Current System, *Deep Sea Res. Part II Top. Stud. Oceanogr.*, *54*(8-10), 837–858, doi:10.1016/j.dsr2.2007.02.003.

Morrow, R., F. Fang, M. Fieux, and R. Molcard (2003), Anatomy of three warm-core Leeuwin Current eddies, *Deep Sea Res. Part II Top. Stud. Oceanogr.*, *50*(12-13), 2229–2243, doi:10.1016/S0967-0645(03)00054-7.

Morrow, R., F. Birol, D. Griffin, and J. Sudre (2004), Divergent pathways of cylonic and anti-cyclonic ocean eddies, *Geophys. Res. Lett.*, *31*(24), 1–5, doi:10.1029/2004GL020974.

Paris, C. B., J. Helgers, E. van Sebille, and A. Srinivasan (2013), Connectivity Modeling System: A probabilistic modeling tool for the multi-scale tracking of biotic and abiotic variability in the ocean, *Environ. Model. Softw.*, *42*, 47–54, doi:10.1016/j.envsoft.2012.12.006.

Pearce, A., and M. Feng (2007), Observations of warming on the Western Australian continental shelf, *Mar. Freshw. Res.*, *58*(10), 914, doi:10.1071/MF07082.

Pearce, A., and C. Pattiaratchi (1998), The Capes Current: a summer countercurrent flowing past Cape Leeuwin and Cape Naturaliste, Western Australia, *Cont. Shelf Res.*, *19*(3), 401–420, doi:10.1016/S0278-4343(98)00089-2.

Rhein, M. et al. (2013), 2013: Observations: Ocean, in *Climate Change 2013: The Physical Science Basis. Contribution of Working Group I to the Fifth Assessment Report of the Intergovernmental Panel on Climate Change*, edited by V. B. and P. M. M. Stocker, T.F., D. Qin, G.-K. Plattner, M. Tignor, S.K. Allen, J. Boschung, A. Nauels, Y. Xia, pp. 255–315, Cambridge University Press, United Kingdom and New York, NY, USA.

Ridgway, K. R., and S. A. Condie (2004), The 5500-km-long boundary flow off western and southern Australia, *J. Geophys. Res.*, *109*(C4), C04017, doi:10.1029/2003JC001921.

Ridgway, K. R., and J. S. Godfrey (2015), The source of the Leeuwin Current seasonality, *J. Geophys. Res. Ocean.*, *6843–6864*(120), doi:10.1002/2015JC011049.

Saraceno, M., P. T. Strub, and P. M. Kosro (2008), Estimates of sea surface height and near-surface alongshore coastal currents from combinations of altimeters and tide gauges, *J. Geophys. Res. Ocean.*, *113*(11), 1–20, doi:10.1029/2008JC004756.

Schloesser, F. (2014), A Dynamical Model for the Leeuwin Undercurrent, *J. Phys. Oceanogr.*, *44*(7), 1798–1810, doi:10.1175/JPO-D-13-0226.1.

Schwarzkopf, F. U., and C. W. Böning (2011), Contribution of Pacific wind stress to multi-decadal variations in upper-ocean heat content and sea level in the tropical south Indian Ocean, *Geophys. Res. Lett.*, *38*(12), n/a–n/a, doi:10.1029/2011GL047651.

van Sebille, E., P. J. van Leeuwen, A. Biastoch, and W. P. M. de Ruijter (2010), Flux comparison of Eulerian and Lagrangian estimates of Agulhas leakage: A case study using a numerical model, *Deep Sea Res. Part I Oceanogr. Res. Pap.*, *57*(3), 319–327, doi:10.1016/j.dsr.2009.12.006.

van Sebille, E., M. H. England, J. D. Zika, and B. M. Sloyan (2012), Tasman leakage in a fine-resolution ocean model, *Geophys. Res. Lett.*, *39*(6), doi:10.1029/2012GL051004.

van Sebille, E., P. Spence, M. R. Mazloff, M. H. England, S. R. Rintoul, and O. a. Saenko (2013), Abyssal connections of Antarctic Bottom Water in a Southern Ocean State Estimate, *Geophys. Res. Lett.*, *40*(December 2007), doi:10.1002/grl.50483.

van Sebille, E., J. Sprintall, F. U. Schwarzkopf, A. Sen Gupta, A. Santoso, M. H. England, A. Biastoch, and C. W. Böning (2014), Pacific to Indian Ocean connectivity: Tasman leakage, Indonesian Throughflow, and the role of ENSO, *J. Geophys. Res. Ocean.*, *119*(2), 1365–1382.

Siedler, G., M. Rouault, and J. R. E. Lutjeharms (2006), Structure and origin of the subtropical South Indian Ocean Countercurrent, *Geophys. Res. Lett.*, *33*(24), L24609, doi:10.1029/2006GL027399.

Smith, R., A. Huyer, J. S. Godfrey, and J. A. Church (1991), The Leeuwin current off western Australia, 1986-1987, *J. Phys. …*, (21), 323–345.

Speich, S., B. Blanke, P. De Vries, S. Drijfhouté, K. Döös, and A. Ganachaud (2002), Tasman leakage : A new route in the global ocean conveyor belt Tasman leakage : a new route in the global ocean conveyor belt, *Geophys. Res. Lett.*, *29*(May).

Sun, C., M. Feng, R. J. Matear, M. a. Chamberlain, P. Craig, K. R. Ridgway, and A. Schiller (2012), Marine Downscaling of a Future Climate Scenario for Australian Boundary

Currents, *J. Clim.*, *25*(8), 2947–2962, doi:10.1175/JCLI-D-11-00159.1.

Thompson, P. a., P. Bonham, P. Thomson, W. Rochester, M. a. Doblin, A. M. Waite, A. Richardson, and C. S. Rousseaux (2015), Climate variability drives plankton community composition changes: the 2010–2011 El Niño to La Niña transition around Australia, *J. Plankton Res.*, *37*(5), 966–984, doi:10.1093/plankt/fbv069.

Waite, A. M. et al. (2007), The Leeuwin Current and its eddies: An introductory overview, *Deep Sea Res. Part II Top. Stud. Oceanogr.*, *54*(8-10), 789–796, doi:10.1016/j.dsr2.2006.12.008.

Wang, M., R. O'Rorke, a. M. Waite, L. E. Beckley, P. Thompson, and a. G. Jeffs (2015), Condition of larvae of western rock lobster (Panulirus cygnus) in cyclonic and anticyclonic eddies of the Leeuwin Current off Western Australia, *Mar. Freshw. Res.*, *122*, 1158–1167, doi:10.1016/j.pocean.2014.01.003.

Wernberg, T., B. Russell, P. J. Moore, S. D. Ling, D. a. Smale, A. Campbell, M. a. Coleman, P. D. Steinberg, G. a. Kendrick, and S. D. Connell (2011), Impacts of climate change in a global hotspot for temperate marine biodiversity and ocean warming, *J. Exp. Mar. Bio. Ecol.*, *400*(1-2), 7–16, doi:10.1016/j.jembe.2011.02.021.

Woo, M., and C. Pattiaratchi (2008), Hydrography and water masses off the western Australian coast, *Deep Sea Res. Part I Oceanogr. Res. Pap.*, *55*(9), 1090–1104, doi:10.1016/j.dsr.2008.05.005.

Woo, M., C. Pattiaratchi, and W. Schroeder (2006), Dynamics of the Ningaloo Current off Point Cloates, Western Australia, *Mar. Freshw. Res.*, *57*(3), 291, doi:10.1071/MF05106.

Xu, J., R. J. Lowe, G. N. Ivey, N. L. Jones, and R. Brinkman (2015), Observations of the shelf circulation dynamics along Ningaloo Reef, Western Australia during the austral spring and summer, *Cont. Shelf Res.*, *95*, 54–73, doi:10.1016/j.csr.2014.12.013.

7 Figures

See 2015JC011486-p01.pdf

Figure 1. Evaluation of the TROPAC01 model: comparing the model sea surface height data for the period 1993–2009 to AVISO altimetry data over the same period. (a)-(c) comparison of mean sea surface height. (d)-(f) comparison of sea surface height variability, computed as the local root-mean-square variance of the sea surface height time series.

See 2015JC011486-f02.pdf

Figure 2. Mean (upper left) and bimonthly mean (1960-2009) meridional velocity (m/s) at 32°S in the TROPAC01 model. Contours are 0.04 m/s and only negative velocities are shown.

See 2015JC011486-p03.pdf

Figure 3. Eulerian southward transport from TROPAC01 at 32°S for years 1960-2009. Bar colours are different groupings of levels from TROPAC01.

See 2015JC011486-p04.pdf

Figure 4. Connectivity map between the northern offshore/Indonesian Throughflow particles and the Leeuwin Current region as diagnosed from Lagrangian trajectories. The proportion of transport in each 0.5° × 0.5° degree grid cell from trajectories that entered the Leeuwin Current region (blue) and trajectories that did not (red). Any blue value above 50% indicates that grid cell was dominated by trajectories that entered the Leeuwin Current region. The Leeuwin Current region is defined as any sectors pictured by the thick black lines. This figure demonstrates the importance of the Leeuwin Current as a pathway for water between the northern offshore region/Indonesian Throughflow and Australia's mid-latitude and South Australian coastlines.

See 2015JC011486-p05.pdf

Figure 5. Source water exchange along the Leeuwin Current's pathway. Numbers are transport (Sv) across the pictured sector boundaries (black lines), taking the average for years 1966-2003 and depth-integrating to 300m. Orange arrows are particles originating from the Indonesian Throughflow region, purple arrows are from the northern offshore section and green arrows from the western offshore section. Size and direction of arrows are indicative of transport size and direction of flow, respectively.

See 2015JC011486-p06.pdf

Figure 6. Mean seasonal contribution of Leeuwin Current sources along the Leeuwin Current's downstream flow, as located by the coral arrows in the maps on the right, for each row. Units are in Sv and the mean is taken over the years 1966-2003 and depth-integrating to 300m. Orange lines are particles originating from the Indonesian Throughflow region, purple lines are from the northern offshore section and green lines from the western offshore section. The black lines are the totals of the three coloured lines.

See 2015JC011486-p07.pdf

Figure 7. Depth-horizontal space transport sections along the Leeuwin Current's downstream flow. Plots (a)-(b) are in depth-longitude space, contoured transport is the water leaving sectors 1 and 2, respectively. Similarly, plots (c)-(e) show transport due to water leaving sectors 3, 4 and 5 (respectively) but now in depth-latitude space. Contour intervals are 0.01 Sv where results have been binned to 0.25 degrees and 50 metres for horizontal and depth space, respectively. Orange lines are particles originating from the Indonesian Throughflow region, purple lines are from the northern offshore section and green lines from the western offshore section.

See 2015JC011486-p08.pdf

Figure 8. Quantification of direct pathways through the Leeuwin Current region. The bold end of each edge indicates direction of flux. Inshore green edges indicate water that is travelling close to the coast having passed through all preceding inshore sector(s). Offshore red edges quantify trajectories that travelled through all green inshore upstream sector(s) and then exited the system via the red offshore edge. Purple curved edges indicate trajectories that have travelled directly through the previous inshore sector(s) and then recirculated upstream. Units are in Sv and the mean is taken over the years 1966-2003 and depth-integrating to 300m.

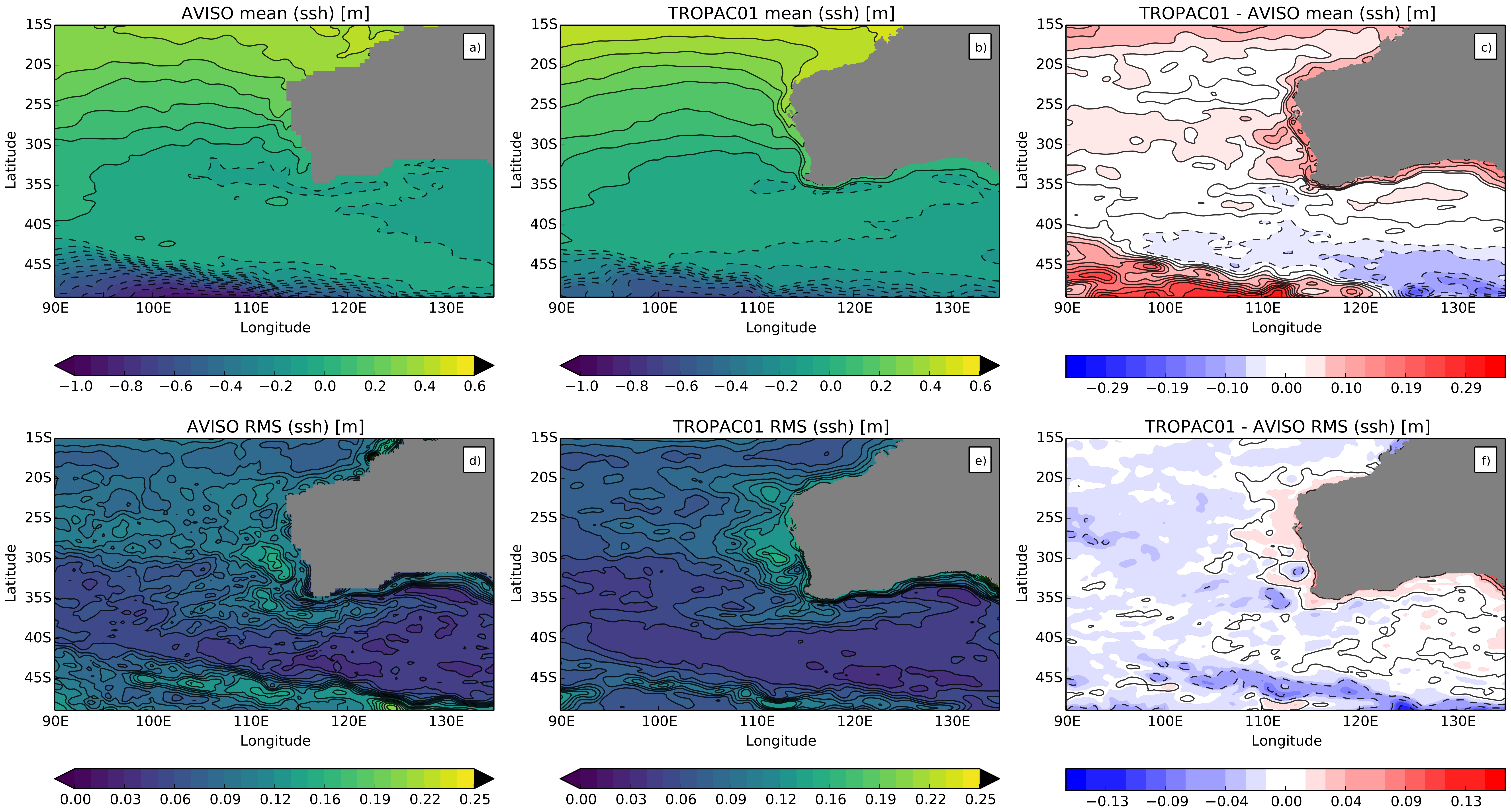
AVISO mean (ssh) [m]
TROPAC01 mean (ssh) [m]
TROPAC01 - AVISO mean (ssh) [m]
AVISO RMS (ssh) [m]
TROPAC01 RMS (ssh) [m]
TROPAC01 - AVISO RMS (ssh) [m]
a)
b)
c)
d)
e)
f)
Latitude
Longitude
15S
20S
25S
30S
35S
40S
45S
90E
100E
110E
120E
130E
−1.0 −0.8 −0.6 −0.4 −0.2 0.0 0.2 0.4 0.6
−0.29 −0.19 −0.10 0.00 0.10 0.19 0.29
0.00 0.03 0.06 0.09 0.12 0.16 0.19 0.22 0.25
−0.13 −0.09 −0.04 0.00 0.04 0.09 0.13

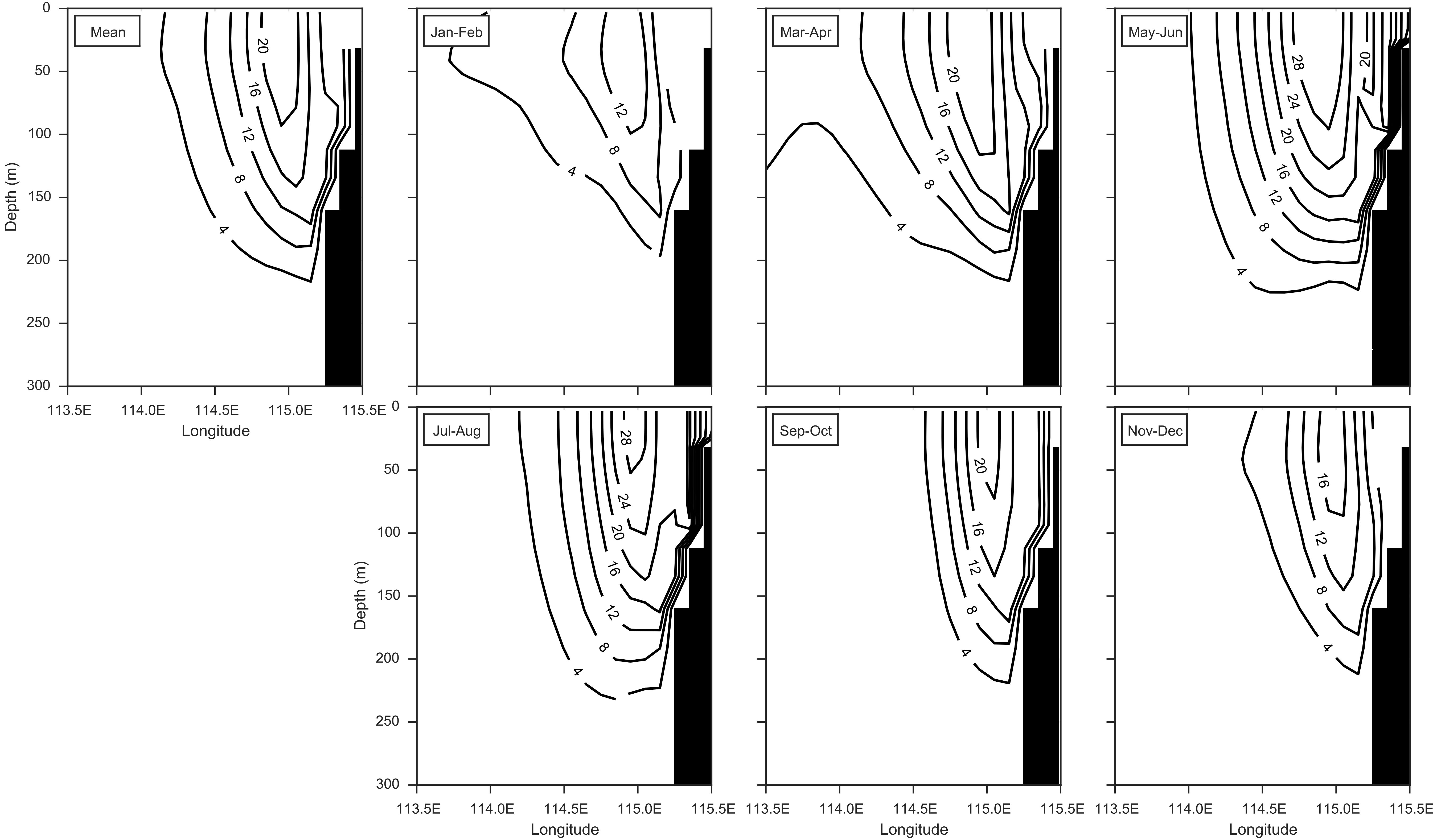
Mean
Jan-Feb
Mar-Apr
May-Jun
Jul-Aug
Sep-Oct
Nov-Dec
Depth (m)
Longitude
0
50
100
150
200
250
300
113.5E
114.0E
114.5E
115.0E
115.5E
4
8
12
16
20
24
28

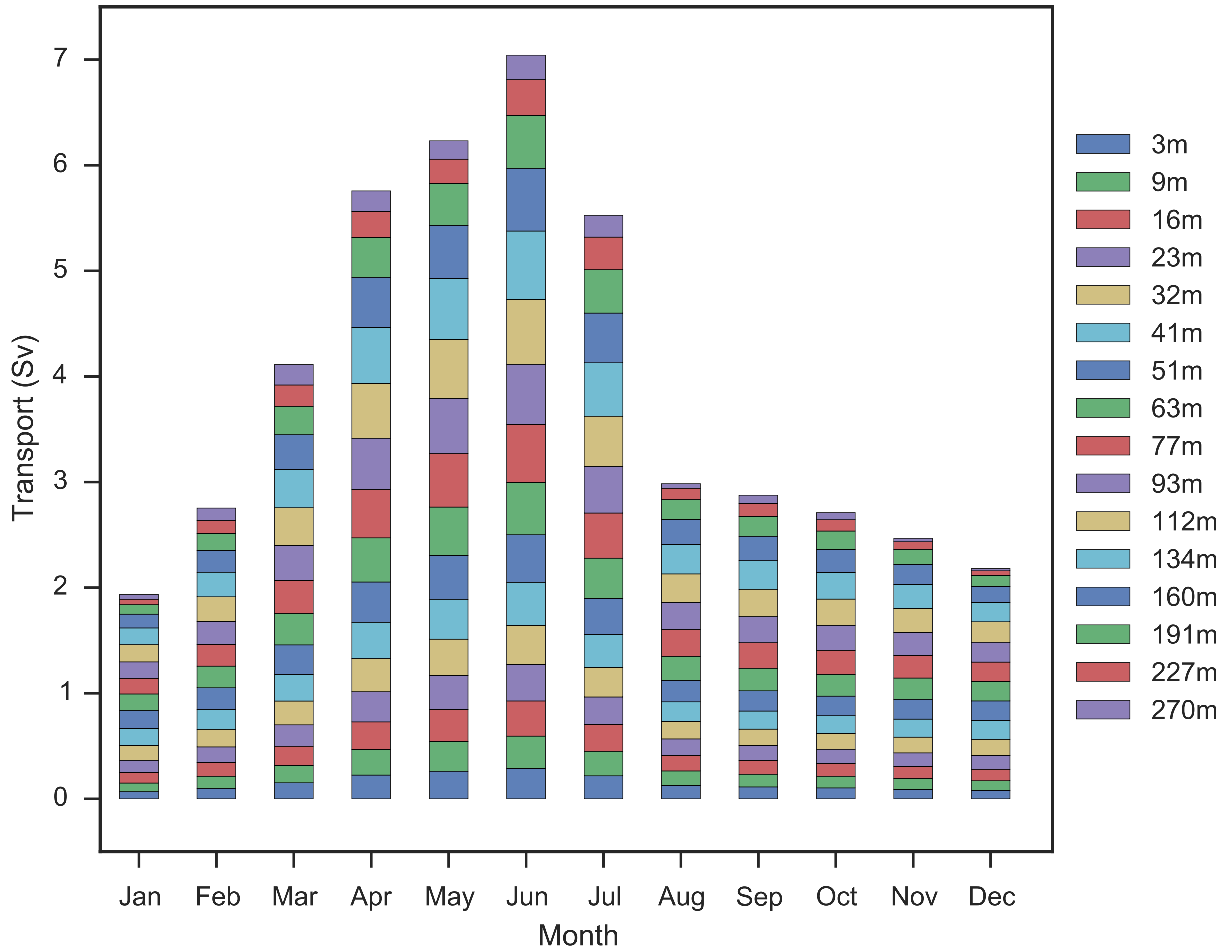

Transport (Sv)
0
1
2
3
4
5
6
7
Jan
Feb
Mar
Apr
May
Jun
Jul
Aug
Sep
Oct
Nov
Dec
Month
3m
9m
16m
23m
32m
41m
51m
63m
77m
93m
112m
134m
160m
191m
227m
270m

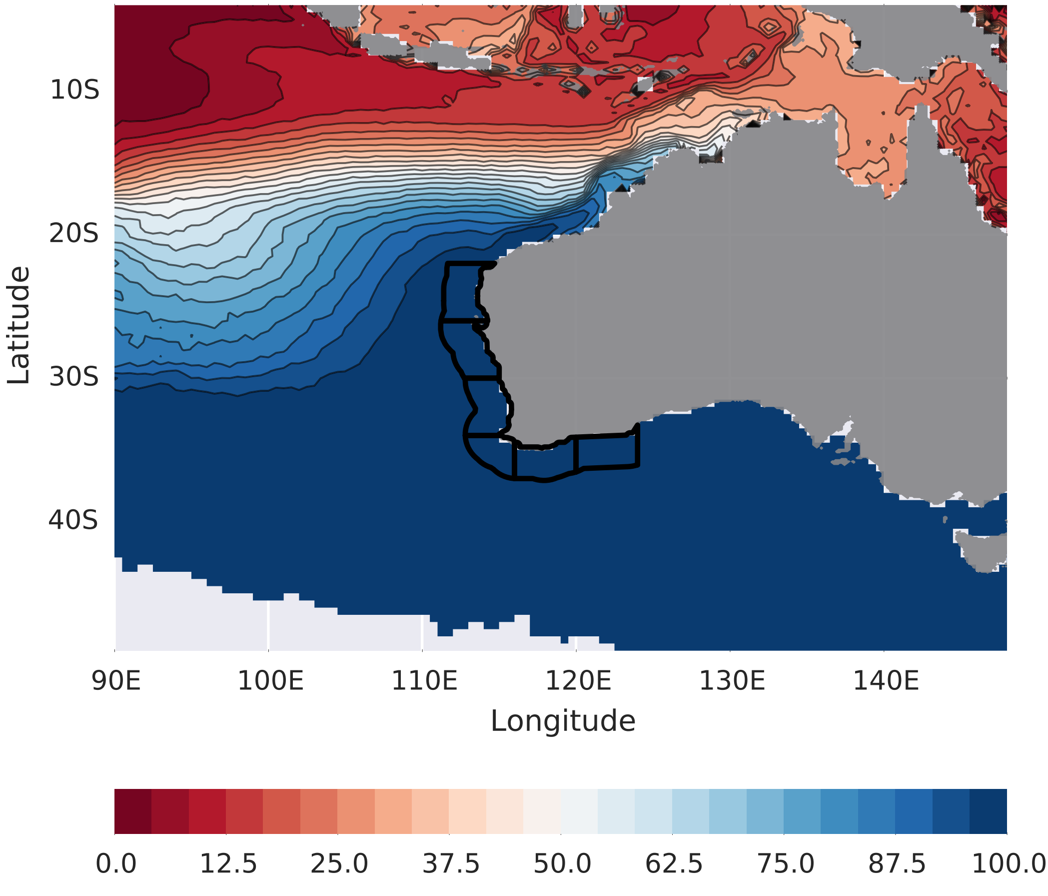

10S
20S
30S
40S
Latitude
90E
100E
110E
120E
130E
140E
Longitude
0.0
12.5
25.0
37.5
50.0
62.5
75.0
87.5
100.0

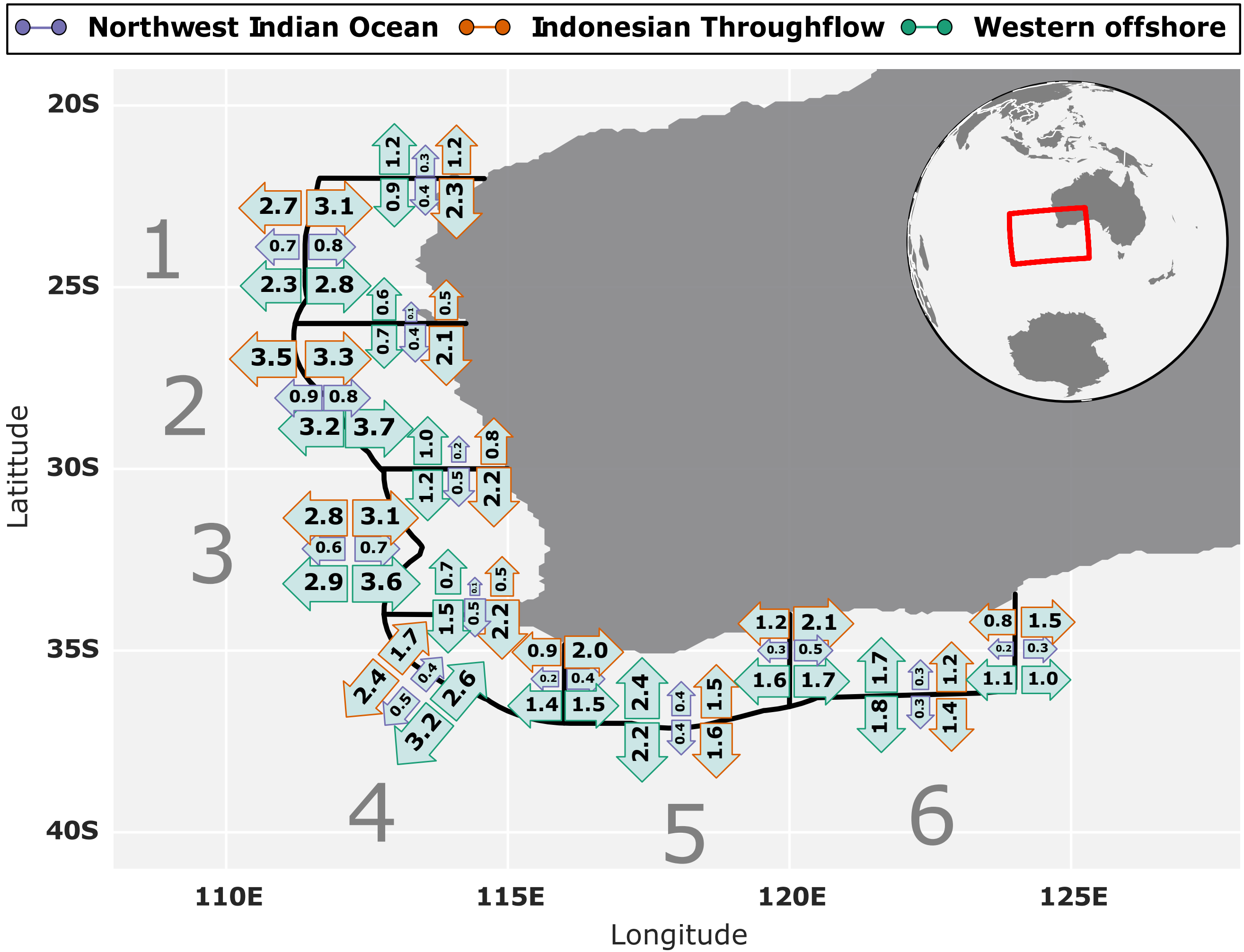

Northwest Indian Ocean
Indonesian Throughflow
Western offshore
20S
25S
30S
35S
40S
110E
115E
120E
125E
Latitude
Longitude
1
2
3
4
5
6
2.7 3.1 1.2 0.3 1.2 0.9 0.4 2.3
0.7 0.8
2.3 2.8 0.6 0.1 0.5 0.7 0.4 2.1
3.5 3.3
0.9 0.8
3.2 3.7 1.0 0.2 0.8 1.2 0.5 2.2
2.8 3.1
0.6 0.7
2.9 3.6 0.7 0.1 0.5 1.5 0.5 2.2
1.7 2.4 0.4 0.5 2.6 3.2
0.9 2.0 0.2 0.4 1.4 1.5
2.4 0.4 1.5 2.2 0.4 1.6
1.2 2.1 0.3 0.5 1.6 1.7
1.7 0.3 1.2 1.8 0.3 1.4
0.8 1.5 0.2 0.3 1.1 1.0

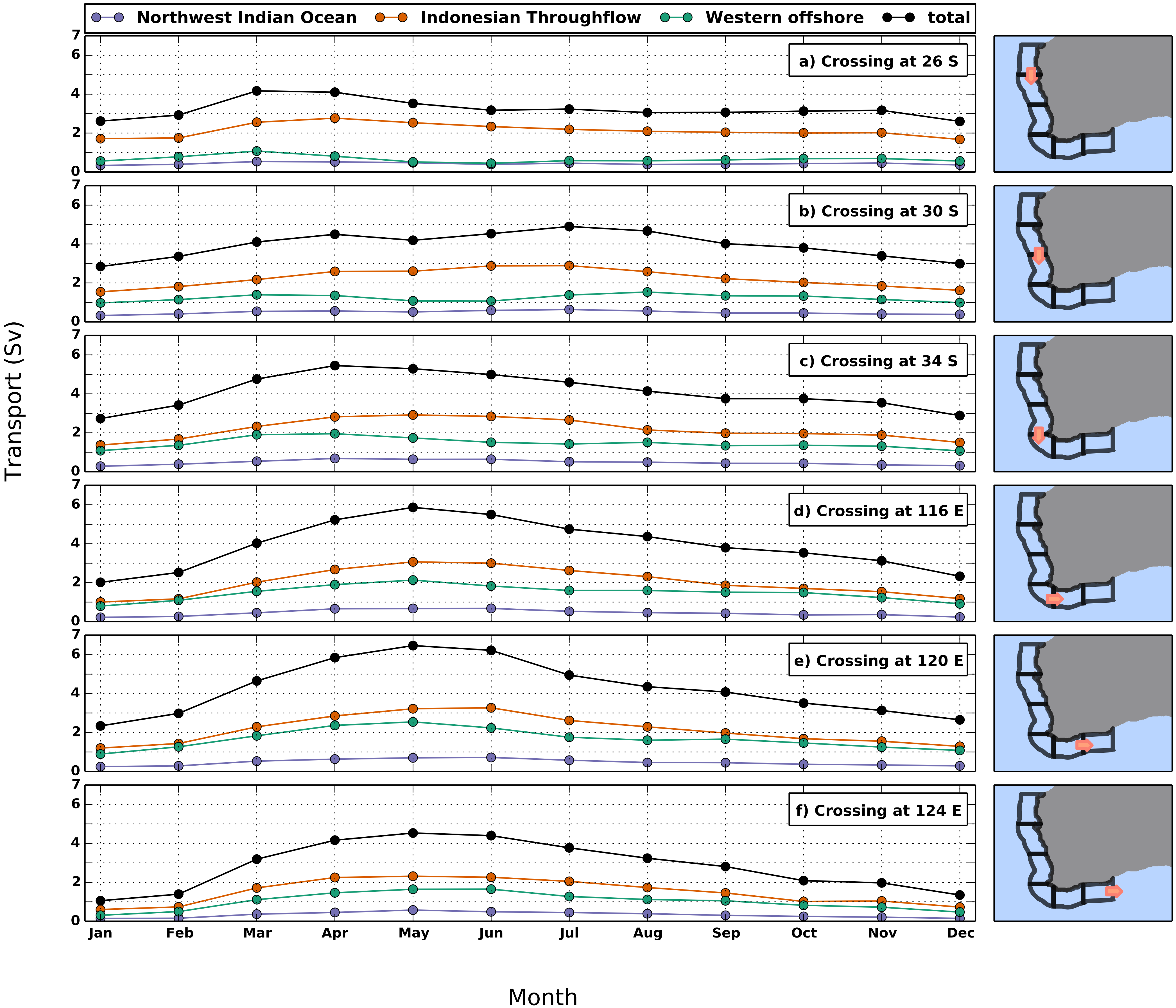
Northwest Indian Ocean
Indonesian Throughflow
Western offshore
total
a) Crossing at 26 S
b) Crossing at 30 S
c) Crossing at 34 S
d) Crossing at 116 E
e) Crossing at 120 E
f) Crossing at 124 E
Transport (Sv)
Month
Jan
Feb
Mar
Apr
May
Jun
Jul
Aug
Sep
Oct
Nov
Dec

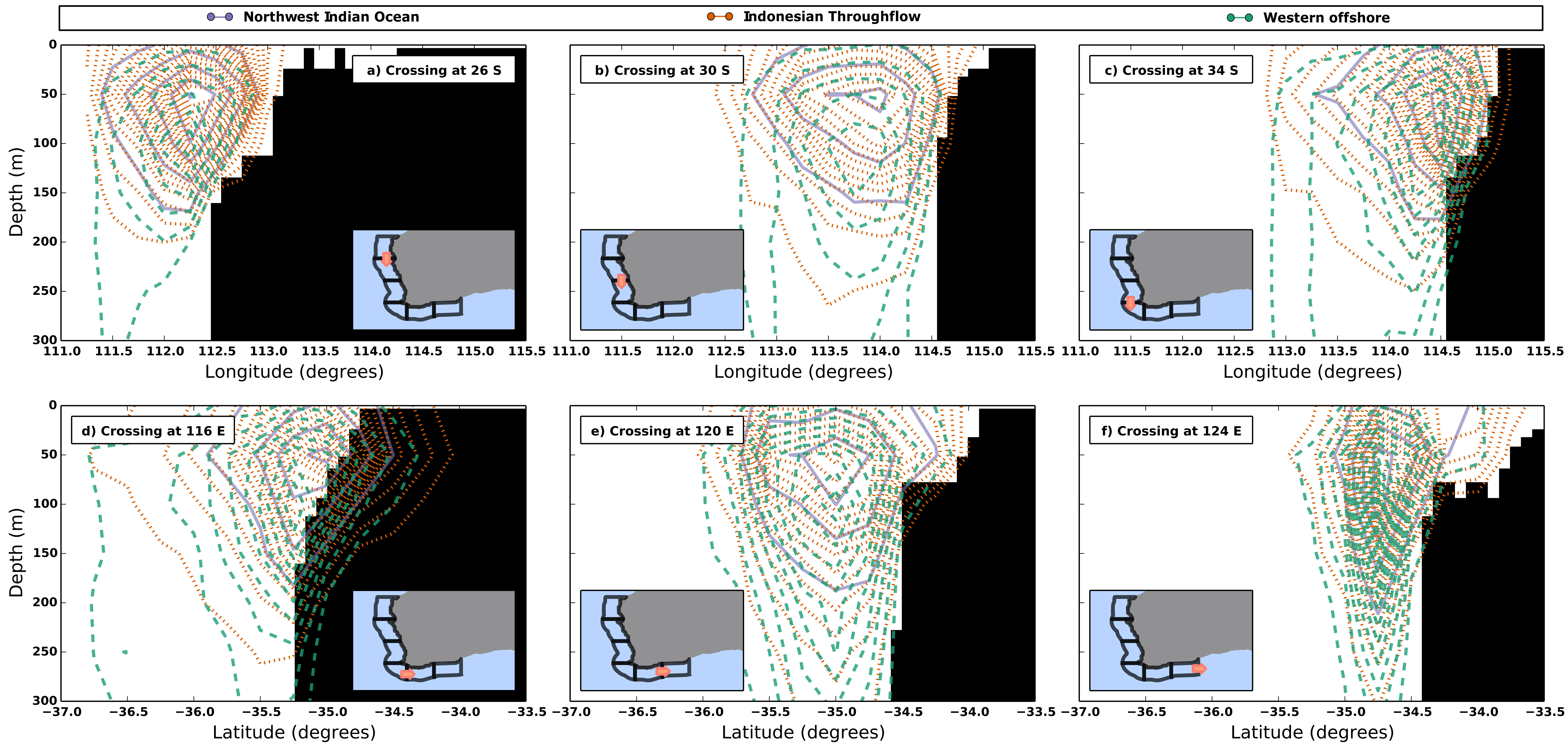

Northwest Indian Ocean
Indonesian Throughflow
Western offshore
a) Crossing at 26 S
b) Crossing at 30 S
c) Crossing at 34 S
d) Crossing at 116 E
e) Crossing at 120 E
f) Crossing at 124 E
Depth (m)
Longitude (degrees)
Latitude (degrees)

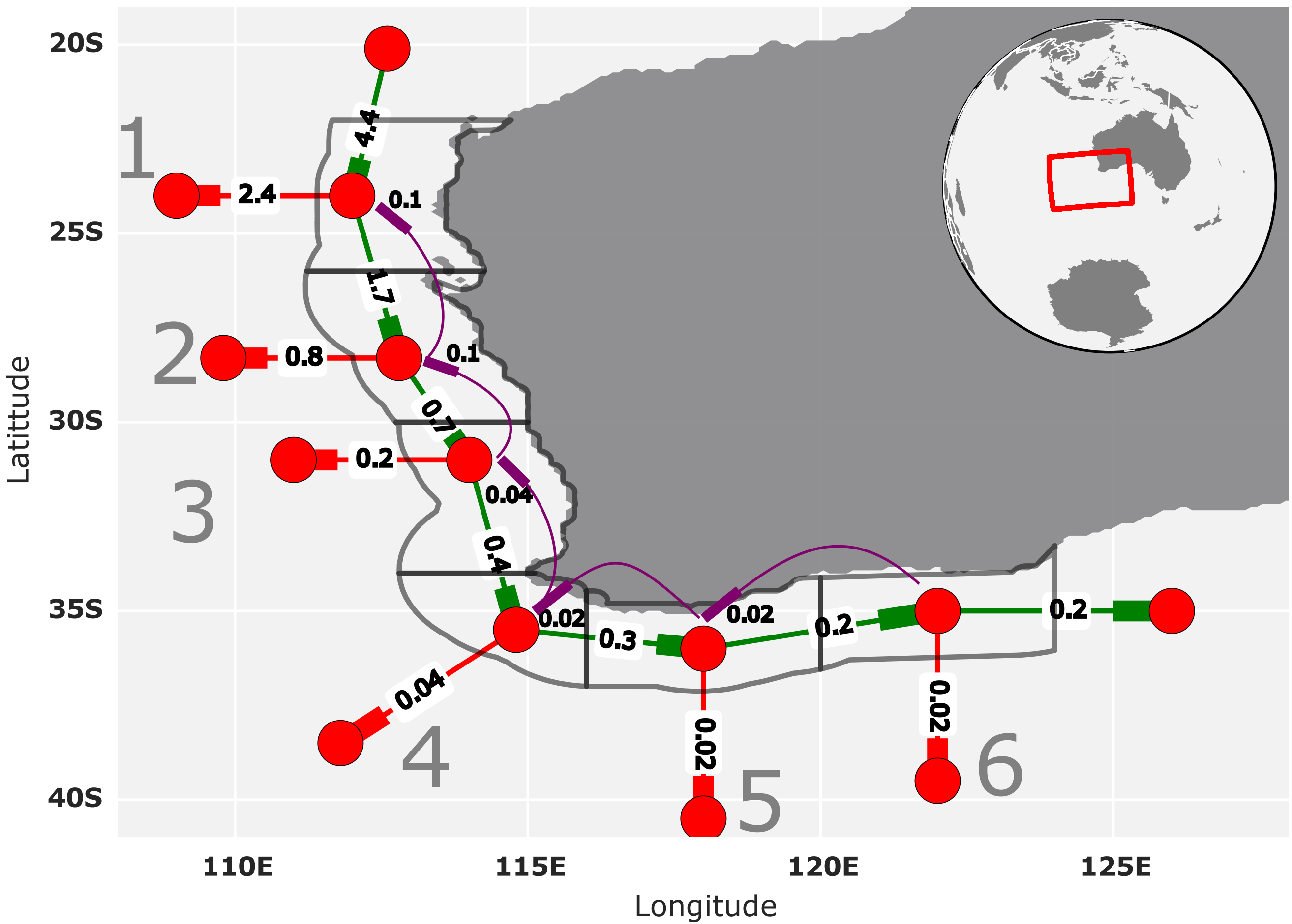

20S
25S
30S
35S
40S
110E
115E
120E
125E
Latititude
Longitude
1
2
3
4
5
6
4.4
2.4
0.1
1.7
0.8
0.1
0.7
0.2
0.04
0.4
0.02
0.3
0.02
0.2
0.2
0.04
0.02
0.02